Delayed Fluorescence from Inverted Singlet and Triplet Excited States for Efficient Organic Light-Emitting Diodes

Daigo Miyajima (daigo.miyajima@riken.jp)
RIKEN https://orcid.org/0000-0002-9578-7349

Naoya Aizawa
RIKEN

Yong-Jin Pu
RIKEN Center for Emergent Matter Science (CEMS) https://orcid.org/0000-0003-3841-2417

Atsuko Nihonyanagi
RIKEN

Ryotaro Ibuka
RIKEN

Hiroyuki Inuzuka
RIKEN

Barun Dhara
RIKEN

Yuki Koyama
RIKEN

Fumito Araoka
RIKEN Center for Emergent Matter Science https://orcid.org/0000-0002-9387-6081

Physical Sciences - Article

Keywords: light-emitting diodes, Hund's multiplicity rule, optoelectronic devices

Posted Date: May 13th, 2021

DOI: https://doi.org/10.21203/rs.3.rs-478258/v1

Version of Record: A version of this preprint was published at Nature on September 14th, 2022. See the published version at https://doi.org/10.1038/s41586-022-05132-y.

Abstract

Hund's multiplicity rule states that for a given electronic configuration, a higher spin state has a lower energy. Rephrasing this rule for molecular excited states predicts a positive energy gap between spin-singlet and spin-triplet excited states, which has been consistent with numerous experimental observations over almost a century. Here, we report a fluorescent molecule that disobeys Hund's rule, possessing a negative singlet–triplet energy gap of −11 meV. The energy inversion of the singlet and triplet excited states results in delayed fluorescence with short time constants of 0.2 μs, which anomalously decrease with decreasing temperature due to the emissive singlet character of the lowest-energy excited state. Organic light-emitting diodes using this molecule exhibited a fast transient electroluminescence decay with a peak external quantum efficiency of 17%, demonstrating potential implications for optoelectronic devices, including displays, lighting, and lasers.

Main Text

The spin multiplicity of molecular excited states plays a crucial role in organic optoelectronic devices. In the case of organic light-emitting diodes (OLEDs), the recombination of charge carriers leads to the formation of singlet and triplet excited states in a 1:3 ratio. This spin statistic limits the internal quantum efficiency of OLEDs and leads to energy loss due to the spin-forbidden nature of triplet excited states to emit photons. To overcome this issue, two strategies have been established for harvesting photons from the 'dark' triplet excited states. The first relies on organometallic complexes with transition metals, such as iridium and platinum, which induce a large spin–orbit coupling to allow triplet states to emit photons as phosphorescence[2–4]. The other utilizes organic molecules that exhibit thermally activated delayed fluorescence (TADF)[5–7]. This class of materials has energetically close singlet and triplet excited states, where ambient thermal energy upconverts the triplet states into singlet states through reverse intersystem crossing (RISC). Although the concept of TADF has the advantage of eliminating the need for transition metals, the resultant temporally delayed fluorescence typically has a time constant in the microsecond or even millisecond range, which is long enough for detrimental bimolecular annihilations, such as triplet–triplet annihilation and triplet–polaron annihilation, to compete with delayed fluorescence. These bimolecular annihilations lead to a decrease in device efficiency under high current densities, known as efficiency roll-off in OLEDs[8,9], and generate high-energy excitons that are suspected to cause chemical degradation of materials, particularly in blue OLEDs[10,11]. The research community has thus focused on minimizing the singlet–triplet energy gap (ΔE_{ST}) to accelerate upconversion by thermal activation[7]. Alternatively, an ideal case would be thermodynamically favourable downconversion with negative ΔE_{ST}, which is not expected if Hund's multiplicity rule applies to the lowest-energy excited state. Herein, we demonstrate experimental evidence of the existence of highly fluorescent organic molecules that disobey Hund's rule and possess negative ΔE_{ST} for constructing efficient OLEDs.

Numerous observations of positive ΔE_{ST} in molecular excited states are generally understood in terms of the exchange interaction, the quantum-mechanical effect involving Pauli repulsion, which stabilises triplet

states relative to singlet states[12]. DE_{ST} is simply equal to twice the positive exchange energy if the lowest-energy singlet and triplet excited states (S_1 and T_1) have the same single-excitation configuration[13]. Although there is general agreement that DE_{ST} must be positive, the potential for negative DE_{ST} in nitrogen-substituted phenalene analogues, such as cycl[3.3.3]azine and heptazine has been discussed during the last two decades[14–20]. Recent theoretical studies have also suggested the possibility of negative DE_{ST} in these molecules by accounting for double-excitation configurations where two electrons of occupied orbitals have been promoted out to virtual orbitals (Supplementary Fig. 1)[16–20]. Because the Pauli exclusion principle restricts the accessible double-excitation configurations in T_1, an effective admixture of such configurations stabilises S_1 relative to T_1. If this stabilisation overcomes the exchange energy, DE_{ST} could have a negative value (Fig. 1a). However, to the best of our knowledge, none of the molecules have been experimentally identified with negative DE_{ST} and the resultant delayed fluorescence from inverted singlet and triplet excited states (DFIST).

Pioneering computational calculations[16] inspired us to focus on heptazine as a potential class of molecules that exhibit DFIST. Correlated wave function theories suggested that S_1 of heptazine lies 0.2–0.3 eV below T_1, though S_1 is a 'dark' state, meaning that the electronic transition to the ground state (S_0) is dipole-forbidden and the oscillator strength (*f*) is zero in the D_{3h} symmetry point group. Interestingly, the heptazine core is shared by several synthesised molecules that exhibit intense TADF with positive DE_{ST}[21–24]. We thus hypothesized that appropriate chemical substitutions would lead to heptazine analogues with negative DE_{ST} and sufficient *f* for intense fluorescence. As such, we introduced 186 different substituents to heptazine to generate 34,596 candidate molecules for computational screening. The structures of all substituents are available in Supplementary Fig. 2. To ensure synthetic feasibility, at most two distinct types of substituents were introduced to the heptazine core, R_1 and R_2 (Fig. 1b). We used standard linear-response time-dependent density functional theory (TDDFT) to calculate DE_{ST} and *f*, which are more affordable in computational cost than those calculated by correlated wave function theories. While the commonly used adiabatic approximation in TDDFT does not account for double-excitation character[17,25], the properties calculated by TDDFT are still useful for pre-screening to narrow the list of candidate molecules prior to high-cost calculations and experimental evaluation, as both S_1 and T_1 of heptazine are almost entirely dominated by the single-excitation configuration between the highest occupied molecular orbital (HOMO) and the lowest unoccupied molecular orbital (LUMO)[16].

Fig. 1c shows the statistics of the screened molecules as a function of DE_{ST} and *f* calculated by TDDFT. A well-known trade-off between small DE_{ST} and large *f* is evident from this particular data set of heptazine analogues. While balancing this trade-off is a key concern in recent synthetic efforts on TADF materials, Fig. 1c demonstrates the optimal combinations of DE_{ST} and *f*, for which one parameter cannot be further improved without sacrificing the other. Fig. 1d further visualizes the trade-off between DE_{ST} and *f* for each fluorescence colour. The screening data suggest 5,264 promising candidates to display fluorescence across the entire visible spectrum with DE_{ST} < 0.35 eV and $f > 0.01$. Setting the range of the

S_1–S_0 energy gap to 2.70–2.85 eV for blue fluorescence further narrows down the candidates to 1,028 molecules, corresponding to 2.97% of all screened molecules. We then assessed their synthetic feasibility and selected two heptazine analogues, $HzTFEX_2$ and $HzPipX_2$ (Fig. 2a), for further evaluation. We note that the unsymmetrical substitutions in these molecules recover f while retaining small $D E_{ST}$ (f = 0.010, 0.015 and $D E_{ST}$ = 210, 334 meV for $HzTFEX_2$ and $HzPipX_2$, respectively).

To examine whether $HzTFEX_2$ and $HzPipX_2$ could have negative $D E_{ST}$, we computed their S_1 and T_1 by correlated wave function theories. Equation-of-motion coupled cluster with single and double excitation (EOM-CCSD)[26] calculations predict that $HzTFEX_2$ possesses a negative $D E_{ST}$ of −12 meV, affirming its potential for exhibiting DFIST. In comparison, the value of $D E_{ST}$ calculated for $HzPipX_2$ remains at a positive value of 10 meV, which is comparable to those of the current state-of-the-art TADF materials[27–38]. Figs. 2b, c show the dominant pair of natural transition orbitals (NTOs)[39] for S_1 and T_1. In both molecules, the hole orbitals are exclusively localized on the peripherical six nitrogen atoms of the heptazine core, whereas the electron orbitals are localized on the central nitrogen atom and the carbon atoms of the core, as well as on the substituents. The spatial separation of these orbitals indicates that the exchange interaction is weak, resulting in nearly degenerate S_1 and T_1 in the single-excitation scenario. In this situation, the stabilisation of S_1 by including the double-excitation configurations becomes more dominant in determining the sign of $D E_{ST}$. Indeed, S_1 of both molecules comprises double-excitation configurations with weights of approximately 1%, which are slightly higher than those of T_1. Two other wave-function-based calculations using second-order algebraic diagrammatic construction (ADC(2))[40] and complete active space with second-order perturbation theory (CASPT2)[41] further validate the inversion of S_1 and T_1 in $HzTFEX_2$ with calculated $D E_{ST}$ values of −34 meV and −184 meV, respectively. However, for $HzPipX_2$, the two methods also invert $D E_{ST}$ (−12 meV with ADC(2) and −171 meV with CASPT2) compared to the positive value of 10 meV predicted with EOM-CCSD (Supplementary Table 1). This variation in the estimates of $D E_{ST}$ highlights the current limitations of excited-state calculations and demands conclusive experimental evaluation.

$HzTFEX_2$ and $HzPipX_2$ were synthesised by nucleophilic aromatic substitution of 2,5,8-trichloroheptazine with the corresponding alcohol or amine, followed by Friedel–Crafts reactions with *m*-xylene. The details of the synthesis and characterisation are given in the Supplementary Information. The photophysical properties of the two molecules were evaluated in deaerated toluene solutions (Fig. 3a, Extended Data Table 1). The steady-state absorption spectra of $HzTFEX_2$ and $HzPipX_2$ comprise the lowest-energy absorption bands centred at 441 nm and 429 nm, respectively, with small molar absorption coefficients on the order of 10^3 M^{-1} cm^{-1}, reflecting the spatial separation between the hole and electron NTOs computed for S_1 of each molecule. Upon photoexcitation, $HzTFEX_2$ exhibits blue emission with a peak wavelength (l_{PL}) of 449 nm and a PL quantum yield (F_{PL}) of 74%, while a slightly blueshifted l_{PL} of 442 nm and a similar F_{PL} of 67% are observed for $HzPipX_2$. These energy differences in absorption and emission are also predicted by TDDFT calculations and are attributed to the piperidyl group in $HzPipX_2$

having a stronger electron-donating effect than the 2,2,2-trifluoroethoxy group in $HzTFEX_2$. In aerated toluene solutions, the F_{PL} values of $HzTFEX_2$ and $HzPipX_2$ decreased to 54% and 37%, respectively. Since atmospheric O_2 can quench molecular triplet excited states, we ascribe the blue emissions of the two molecules at least partially to delayed fluorescence through forward intersystem crossing (ISC) and RISC between S_1 and T_1. This assumption is supported by transient absorption decay measurements on $HzTFEX_2$, which probed ISC from S_1 to T_1 as the signal decay of S_1 at 700 nm and the signal growth of T_1 at 1,600 nm, followed by the persistent signal decays of both S_1 and T_1 (Extended Data Fig. 1). We also note that both decays have similar time constants (223 ns for S_1 and 210 ns for T_1), indicating steady-state conditions with the constant population ratio maintained by ISC and RISC.

To reveal the excited-state kinetics of the two molecules in detail, we performed transient PL decay measurements at varying temperatures (Figs. 3b, c). Both molecules exhibited biexponential transient PL decays, which comprise nanosecond-order prompt fluorescence followed by sub-microsecond delayed fluorescence with temperature-dependent time constants. Remarkably, the time constant of delayed fluorescence (t_{DF}) of $HzTFEX_2$ gradually decreased from 217 ns to 195 ns with decreasing temperature from 300 K to 200 K (Fig. 3d). This anomalous temperature dependence of t_{DF} indicates that S_1 lies energetically below T_1, where lowering the temperature shifts the steady-state population towards emissive S_1 relative to dark T_1 and thus accelerates the delayed fluorescence (i.e., decreases t_{DF}). In comparison, the t_{DF} of $HzPipX_2$ increased from 565 ns to 1,372 ns during the same temperature lowering, as has been similarly observed in conventional TADF materials[5–7]. It is worth noting that the t_{DF} of $HzTFEX_2$ is much shorter than the emission time constants ever reported for TADF materials[27–38] and phosphorescent materials[2–4] used for efficient OLEDs, which are typically in the microsecond range.

We further analysed the temperature-dependent PL decay kinetics with the underlying rate equation. In the absence of phosphorescence and non-radiative decay of T_1 to S_0, the rate equation for the populations of S_1 and T_1 is given by

$$\frac{d}{dt}\begin{pmatrix} S_1 \\ T_1 \end{pmatrix} = \begin{pmatrix} -(k_r + k_{nr} + k_{ISC}) & k_{RISC} \\ k_{ISC} & -k_{RISC} \end{pmatrix} \begin{pmatrix} S_1 \\ T_1 \end{pmatrix} \quad (1)$$

where k_r, k_{nr}, k_{ISC}, and k_{RISC} are the rate constants of radiative decay of S_1 to S_0, non-radiative decay of S_1 to S_0, ISC of S_1 to T_1, and RISC of T_1 to S_1, respectively. By numerically fitting Eq. (1) to the PL decay data at 300 K, we found that RISC was faster than ISC in $HzTFEX_2$ (k_{RISC} = 4.2 ´ 10^7 s^{-1} vs k_{ISC} = 2.3 ´ 10^7 s^{-1}) but slower than ISC in $HzPipX_2$ (k_{RISC} = 2.2 ´ 10^7 s^{-1} vs k_{ISC} = 8.9 ´ 10^7 s^{-1}) (Figs. e, f). Furthermore, the temperature dependence of k_{ISC} and k_{RISC} follows the Arrhenius equation, $k = A \exp(-E_a/k_B T)$, where k is the rate constant, A is the pre-exponential factor, E_a is the activation energy, k_B is the Boltzmann constant, and T is the absolute temperature (Extended Data Fig. 2). The best-fit parameters of the Arrhenius equation yield the activation energies of ISC and RISC ($E_{a,ISC}$ and $E_{a,RISC}$) (Extended Data Table 1).

Subtracting $E_{a,ISC}$ from $E_{a,RISC}$, we determined the DE_{ST} of $HzTFEX_2$ to be −11 meV, which is in marked contrast to the positive DE_{ST} values previously observed in numerous molecules including $HzPipX_2$ (DE_{ST} = 52 meV).

Having experimentally determined negative DE_{ST}, we conclude that $HzTFEX_2$ exhibits 'delayed fluorescence from inverted singlet and triplet excited states (DFIST)'. Further synthetic efforts replacing the xylyl groups in $HzTFEX_2$ with either phenyl or tolyl groups led to $HzTFEP_2$ and $HzTFET_2$, which similarly display DFIST with measured DE_{ST} values of −14 meV and −13 meV, respectively (see Extended Data Table 1 and Supplementary Fig. 3 for detail), indicating the potential of heptazines for further developing efficient DFIST materials. Thus, we propose to refer to the present type of emissions as 'H (heptazine)-type delayed fluorescence' by analogy with 'E (eosin)-type delayed fluorescence' referred to as TADF[42] and 'P (pyren)-type delayed fluorescence' involving triplet–triplet annihilation[43].

Finally, we evaluated the electroluminescence (EL) properties of $HzTFEX_2$ in OLEDs fabricated by thermal evaporation. The details of the fabrication procedures and the device structures are given in the Supplementary Information. Figs. 4a and b show the EL spectra, current density–voltage–luminance characteristics, and external quantum efficiency–luminance characteristics of the OLED. Intense blue EL originating from $HzTFEX_2$ was observed with spectral peak wavelengths (l_{PL}) at 450 nm and 479 nm and Commission Internationale de l¢éclairage (CIE) coordinates of (0.17, 0.24). The maximum external quantum efficiency reached 17%, corresponding to an internal quantum efficiency of 80% for a bottom-emission OLED with a typical light-outcoupling efficiency of 20%[44]. We note that the viewing-angle dependence of the luminance followed the Lambertian distribution (Fig. 4b inset), ensuring accurate estimation of the external quantum efficiency from the forward emission. Remarkably, $HzTFEX_2$ exhibited fast transient EL decay, reflecting the sub-microsecond H-type delayed fluorescence (Fig. 4c). In comparison, much slower transient EL decays were observed for the E-type delayed fluorescence of 2,4,5,6-tetra(carbazol-9-yl)isophthalonitrile (4CzIPN)[6] and P-type delayed fluorescence of 2-methyl-9,10-bis(naphthalen-2-yl)anthracene (MADN)[45], though the EL of MADN initially decayed faster by the prompt fluorescence solely from S_1[46]. It is thus evident that the fast triplet harvesting of $HzTFEX_2$ with negative DE_{ST} can be retained even in actual OLEDs. Although the efficiency roll-off in this preliminary device concerning the large hole-injection barrier caused by the high ionization potential of $HzTFEX_2$ (6.3 eV) is still significant, we anticipate that further optimization of molecular design will address this issue and allow a conclusive exploration of the effects of negative DE_{ST} on efficiency roll-off and device stability.

In conclusion, we have demonstrated fluorescent heptazine molecules that possess negative DE_{ST}. We observed their blue delayed fluorescence in both PL and EL with anomalous features: (I) very short decay time constants (t_{DF} ~ 0.2 ms), (II) a decreasing trend in t_{DF} with decreasing temperature, and (III) the rate inversion of RISC and ISC ($k_{RISC} > k_{ISC}$). These features indeed arose from negative DE_{ST} and led to the terminology 'delayed fluorescence from inverted singlet and triplet excited states (DFIST)' or 'H (heptazine)-type delayed fluorescence'. We envisage that further development of DFIST materials will

offer stable and efficient OLEDs based on fast triplet-to-singlet downconversion with great implications for displays, lighting, and lasers.

Methods

Quantum chemical calculations For the 34,596 heptazine molecules, the T_1 geometries were optimised using spin-unrestricted DFT with the LC-BLYP functional and the 6-31G basis set. The vertical excitation energies of S_1 and T_1 were calculated using linear-response TDDFT with the LC-BLYP functional and the 6-31G(d) basis set. The range-separated parameter for the LC-BLYP functional was set to 0.18 $bour^{-1}$ to incorporate a reasonable amount of exact exchange. The T_1 geometries of $HzTFEX_2$ and $HzPipX_2$ were also optimised using spin-unrestricted second-order Møller–Plesset perturbation theory (MP2) with the correlation consistent cc-pVDZ basis set. The vertical excitation energies of S_1 and T_1 at the MP2 geometries of $HzTFEX_2$ and $HzPipX_2$ were calculated using EOM-CCSD[26], ADC(2)[40], and CASPT2[41] with the cc-pVDZ basis set. The CASPT2 calculations were performed with the fully internally contracted scheme over the state-averaged complete active space self-consistent field (CASSCF) wave functions with an active space of 12 electrons and 12 orbitals. The DFT, TDDFT, MP2, and EOM-CCSD calculations were performed using Gaussian 16 RevC.01. The ADC(2) calculations were performed using Q-Chem 5.3.0. The CASSCF and CASPT2 calculations were performed using Orca 4.2.1.

Materials and synthesis Commercially available reagents and solvents were used without further purification unless otherwise noted. 4CzIPN and MADN were purchased from Luminescence Technology Corporation and e-Ray Optoelectronics Technology, respectively. The synthetic procedures and characterization data of the heptazine molecules are detailed in the Supplementary Information.

Photophysical measurements Steady-state UV-vis absorption spectra were recorded on a SHIMADZU UV-3600i Plus spectrophotometer. Steady-state PL spectra were acquired on a HORIBA FL3 spectrofluorometer with 370 nm photoexcitation from a Xe arc lamp. The absolute PL quantum yields were determined using a Hamamatsu Photonics C9920 integrated sphere system with 370 nm excitation from a Xe arc lamp. Transient absorption decay measurements were performed by a randomly interleaved plus train method[47] on a UNISOKU picoTAS system with a 355 nm Q-switched laser pump source (pulse width < 350 ps) and a supercontinuum white probe source (pulse width < 100 ps). Transient PL decay measurements were performed by time-correlated single photon counting on a HORIBA FL3 spectrofluorometer with a 370 nm LED pump source (pulse width < 1.2 ns) and a UNISOKU CoolSpek cryostat using liquid nitrogen as the coolant. Ionization potentials were determined using a RIKEN KEIKI AC-3 ultraviolet photoelectron yield spectrometer.

Analysis of transient PL decay kinetics The time constants of prompt and delayed fluorescence (t_{PF} and t_{DF}) were determined by biexponential decay fitting and deconvolution with the instrument response function. It is common when determining the rate constants of the transitions involved in TADF to assume $k_{ISC} >> k_{RISC}$ such that the contribution of RISC to the prompt fluorescence is negligible[48].

However, this assumption does not hold true for DFIST materials with $k_{RISC} > k_{ISC}$. Thus, $k_r + k_{nr}$, k_{ISC}, and k_{RISC} were determined without assuming $k_{ISC} >> k_{RISC}$ by fitting Eq. (1) to the transient PL decay data using the scipy.integrate.odeint and scipy.optimize.curve_fit functions in Python 3.7[49]. The values of k_r and k_{nr} were determined from $F_{PL} = k_r/(k_r + k_{nr})$, assuming negligible non-radiative decay of T_1 to S_0. The activation energies of ISC and RISC ($E_{a,ISC}$ and $E_{a,RISC}$) were determined by fitting the Arrhenius equation to the temperature dependence of k_{ISC} and k_{RISC}, respectively. DE_{ST} was determined by subtracting $E_{a,ISC}$ from $E_{a,RISC}$.

OLED fabrication and evaluation The fabrication procedures of OLEDs are detailed in the Supplementary Information. EL spectra were recorded using a Hamamatsu Photonics PMA-12 photonic multichannel analyser. Current density–voltage–luminance characteristics were measured using a Konica Minolta CS-200 luminancemeter and a Keithley 2400 source meter. The viewing-angle dependence of luminance was measured using a home-built spectrogoniometer with a Konica Minolta CS-2000 spectroradiometer. Transient EL decay measurements were performed using a home-built setup with a Hamamatsu Photonics H7826 silicon photomultiplier tube (time response =1.5 ns) and an Agilent 33220A function generator for pulse OLED operation (square-wave voltages = 8, –4 V and frequency = 2 kHz)[50].

Declarations

Acknowledgements This work was supported in part by an Industrial Technology Research Grant for Young Researchers from NEDO (Grant No. 09151455 for Y.-J.P.), JST PRESTO (Grant No. 13417316 for Y.-J.P. and JPMJPR17N1 for N.A.), and JSPS KAKENHI (Grant No. 24685029, 17H03103, 20H02554 for Y.-J.P. and 20K15252 for N.A.). The authors thank Dr. Minjun Kim at RIKEN CEMS, Prof. Takayuki Chiba, and Prof. Masakatsu Hirasawa at Yamagata University for their support in OLED fabrication and evaluation. The computations were partially performed using the HOKUSAI Big Waterfall system at RIKEN.

Author contribution N.A. and D.M. conceived the project. N. A. and Y.-J.P. performed the quantum chemical calculations. N. A., H.I., and Y.-J.P. performed the photophysical measurements. N.A., Y.K., and Y.-J.P. fabricated and evaluated the OLEDs. B.D., R.I., H.I., and A.N. performed synthetic experiments and assisted with the characterisation of the synthesised compounds and the analysis of data. N.A., Y.-J.P., F.A. and D.M. designed the experiments, and analysed the data. N.A., Y.-J.P., and D.M. wrote the manuscript.

Competing interests The authors declare no competing interests.

References

1 Hund, F. Zur Deutung verwickelter Spektren, insbesondere der Elemente Scandium bis Nickel. *Z. Phys.* **33**, 345–371 (1925).

2 Baldo, M. A. *et al.* Highly efficient phosphorescent emission from organic electroluminescent devices. *Nature* **395**, 151–154 (1998).

3 Baldo, M., Lamansky, S., Burrows, P., Thompson, M. & Forrest, S. Very high-efficiency green organic light-emitting devices based on electrophosphorescence. *Appl. Phys. Lett.* **75**, 4–6 (1999).

4 Reineke, S. *et al.* White organic light-emitting diodes with fluorescent tube efficiency. *Nature* **459**, 234–238 (2009).

5 Endo, A. *et al.* Efficient up-conversion of triplet excitons into a singlet state and its application for organic light emitting diodes. *Appl. Phys. Lett.* **98**, 083302 (2011).

6 Uoyama, H., Goushi, K., Shizu, K., Nomura, H. & Adachi, C. Highly efficient organic light-emitting diodes from delayed fluorescence. *Nature* **492**, 234–238 (2012).

7 Liu, Y., Li, C., Ren, Z., Yan, S. & Bryce, M. R. All-organic thermally activated delayed fluorescence materials for organic light-emitting diodes. *Nat. Rev. Mater.* **3**, 18020 (2018).

8 Baldo, M. A., Adachi, C. & Forrest, S. R. Transient analysis of organic electrophosphorescence. II. Transient analysis of triplet-triplet annihilation. *Phys. Rev. B* **62**, 10967 (2000).

9 Murawski, C., Leo, K. & Gather, M. C. Efficiency roll-off in organic light-emitting diodes. *Adv. Mater.* **25**, 6801–6827 (2013).

10 Schmidbauer, S., Hohenleutner, A. & König, B. Chemical degradation in organic light-emitting devices: Mechanisms and implications for the design of new materials. *Adv. Mater.* **25**, 2114–2129 (2013).

11 Lee, J. *et al.* Hot excited state management for long-lived blue phosphorescent organic light-emitting diodes. *Nat. Commun.* **8**, 1–9 (2017).

12 Slater, J. C. The theory of complex spectra. *Phys. Rev.* **34**, 1293 (1929).

13 Ziegler, T., Rauk, A. & Baerends, E. J. On the calculation of multiplet energies by the hartree-fock-slater method. *Theor. Chem. Acc.* **43**, 261–271 (1977).

14 Leupin, W. & Wirz, J. Low-lying electronically excited states of cycl [3.3.3]azine, a bridged 12p-perimeter. *J. Am. Chem. Soc.* **102**, 6068–6075 (1980).

15 Leupin, W., Magde, D., Persy, G. & Wirz, J. 1,4,7-Triazacycl[3.3.3]azine: basicity, photoelectron spectrum, photophysical properties. *J. Am. Chem. Soc.* **108**, 17–22 (1986).

16 Ehrmaier, J. *et al.* Singlet–triplet inversion in heptazine and in polymeric carbon nitrides. *J. Phys. Chem. A* **123**, 8099–8108 (2019).

17 de Silva, P. Inverted singlet–triplet gaps and their relevance to thermally activated delayed fluorescence. *J. Phys. Chem. Lett.* **10**, 5674–5679 (2019).

18 Sanz-Rodrigo, J., Ricci, G., Olivier, Y. & Sancho-Garcia, J.-C. Negative Singlet–Triplet Excitation Energy Gap in Triangle-Shaped Molecular Emitters for Efficient Triplet Harvesting. *J. Phys. Chem. A* **125**, 513–522 (2021).

19 Ricci, G., San-Fabián, E., Olivier, Y. & Sancho-García, J.-C. Singlet-triplet excited-state inversion in heptazine and related molecules: assessment of TD-DFT and ab initio methods. *ChemPhysChem* **22**, 553–560 (2021).

20 Pollice, R., Friederich, P., Lavigne, C., dos Passos Gomes, G. & Aspuru-Guzik, A. Organic molecules with inverted gaps between first excited singlet and triplet states and appreciable fluorescence rates. *Matter*, in press (2021). https://doi.org/10.1016/j.matt.2021.02.017

21 Li, J. *et al.* Highly efficient organic light-emitting diode based on a hidden thermally activated delayed fluorescence channel in a heptazine derivative. *Adv. Mater.* **25**, 3319–3323 (2013).

22 Li, J., Zhang, Q., Nomura, H., Miyazaki, H. & Adachi, C. Thermally activated delayed fluorescence from ^{3}nπ* to ^{1}n π* up-conversion and its application to organic light-emitting diodes. *Appl. Phys. Lett.* **105**, 013301 (2014).

23 Galmiche, L., Allain, C., Le, T., Guillot, R. & Audebert, P. Renewing accessible heptazine chemistry: 2,5,8-tris (3, 5-diethyl-pyrazolyl)-heptazine, a new highly soluble heptazine derivative with exchangeable groups, and examples of newly derived heptazines and their physical chemistry. *Chem. Sci.* **10**, 5513–5518 (2019).

24 Le, T., Galmiche, L., Masson, G., Allain, C. & Audebert, P. A straightforward synthesis of a new family of molecules: 2,5,8-trialkoxyheptazines. Application to photoredox catalyzed transformations. *Chem. Commun.* **56**, 10742–10745 (2020).

25 Elliott, P., Goldson, S., Canahui, C. & Maitra, N. T. Perspectives on double-excitations in TDDFT. *Chem. Phys.* **391**, 110–119 (2011).

26 Stanton, J. F. & Bartlett, R. J. The equation of motion coupled-cluster method. A systematic biorthogonal approach to molecular excitation energies, transition probabilities, and excited state properties. *J. Chem. Phys.* **98**, 7029–7039 (1993).

27 Data, P. *et al.* Dibenzo [*a,j*]phenazine-Cored Donor–Acceptor–Donor Compounds as Green-to-Red/NIR Thermally Activated Delayed Fluorescence Organic Light Emitters. *Angew. Chem. Int. Ed.* **55**, 5739–5744 (2016).

28 Di, D. *et al.* High-performance light-emitting diodes based on carbene-metal-amides. *Science* **356**, 159–163 (2017).

29 Zeng, W. *et al.* Achieving Nearly 30% External Quantum Efficiency for Orange–Red Organic Light Emitting Diodes by Employing Thermally Activated Delayed Fluorescence Emitters Composed of 1,8-Naphthalimide-Acridine Hybrids. *Adv. Mater.* **30**, 1704961 (2018).

30 Wu, T.-L. *et al.* Diboron compound-based organic light-emitting diodes with high efficiency and reduced efficiency roll-off. *Nat. Photonics* **12**, 235–240 (2018).

31 Dos Santos, P. L. *et al.* Triazatruxene: A Rigid Central Donor Unit for a D–A_3 Thermally Activated Delayed Fluorescence Material Exhibiting Sub-Microsecond Reverse Intersystem Crossing and Unity Quantum Yield via Multiple Singlet–Triplet State Pairs. *Adv. Sci.* **5**, 1700989 (2018).

32 Kondo, Y. *et al.* Narrowband deep-blue organic light-emitting diode featuring an organoboron-based emitter. *Nat. Photonics* **13**, 678–682 (2019).

33 Hamze, R. *et al.* Eliminating nonradiative decay in Cu(I) emitters: >99% quantum efficiency and microsecond lifetime. *Science* **363**, 601–606 (2019).

34 Kim, J. U. *et al.* Nanosecond-time-scale delayed fluorescence molecule for deep-blue OLEDs with small efficiency rolloff. *Nat. Commun.* **11**, 1–8 (2020).

35 Cui, L.-S. *et al.* Fast spin-flip enables efficient and stable organic electroluminescence from charge-transfer states. *Nat. Photonics* **14**, 636–642 (2020).

36 Wada, Y., Nakagawa, H., Matsumoto, S., Wakisaka, Y. & Kaji, H. Organic light emitters exhibiting very fast reverse intersystem crossing. *Nat. Photonics* **14**, 643–649 (2020).

37 Lim, H. *et al.* Highly Efficient Deep-Blue OLEDs using a TADF Emitter with a Narrow Emission Spectrum and High Horizontal Emitting Dipole Ratio. *Adv. Mater.* **32**, 2004083 (2020).

38 Aizawa, N., Matsumoto, A. & Yasuda, T. Thermal equilibration between singlet and triplet excited states in organic fluorophore for submicrosecond delayed fluorescence. *Sci. Adv.* **7**, eabe5769 (2021).

39 Martin, R. L. Natural transition orbitals. *J. Chem. Phys.* **118**, 4775–4777 (2003).

40 Schirmer, J. Beyond the random-phase approximation: A new approximation scheme for the polarization propagator. *Phys. Rev. A* **26**, 2395 (1982).

41 Andersson, K., Malmqvist, P. Å. & Roos, B. O. Second-order perturbation theory with a complete active space self-consistent field reference function. *J. Chem. Phys.* **96**, 1218–1226 (1992).

42 Parker, C. & Hatchard, C. Triplet-singlet emission in fluid solutions. Phosphorescence of eosin. *Trans. Faraday Soc.* **57**, 1894–1904 (1961).

43 Parker, C. Sensitized P-type delayed fluorescence. *Proc. R. Soc. London Ser. A* **276**, 125–135 (1963).

44 Nowy, S., Krummacher, B.C., Frischeisen, J., Reinke, N.A., Brütting, W. Light extraction and optical loss mechanisms in organic light-emitting diodes: influence of the emitter quantum efficiency. *J. Appl. Phys.* **104**, 123109 (2008).

45 Lee, M.-T., Chen, H.-H., Liao, C.-H., Tsai, C.-H. & Chen, C. H. Stable styrylamine-doped blue organic electroluminescent device based on 2-methyl-9,10-di(2-naphthyl)anthracene. *Appl. Phys. Lett.* **85**, 3301–3303 (2004).

46 Pu, Y.-J. *et al.* Absence of delayed fluorescence and triplet–triplet annihilation in organic light emitting diodes with spatially orthogonal bianthracenes. *J. Mater. Chem. C* **7**, 2541–2547 (2019).

47 Nakagawa, T., Okamoto, K., Hanada, H. & Katoh, R. Probing with randomly interleaved pulse train bridges the gap between ultrafast pump-probe and nanosecond flash photolysis. *Opt. Lett.* **41**, 1498–1501 (2016).

48 Goushi, K., Yoshida, K., Sato, K. & Adachi, C. Organic light-emitting diodes employing efficient reverse intersystem crossing for triplet-to-singlet state conversion. *Nat. Photonics* **6**, 253–258 (2012).

49 Haase, N. *et al.* Kinetic Modeling of Transient Photoluminescence from Thermally Activated Delayed Fluorescence. *J. Phys. Chem. C* **122**, 29173–29179 (2018).

50 Kondakov, D. Characterization of triplet-triplet annihilation in organic light-emitting diodes based on anthracene derivatives. *J. Appl. Phys.* **102**, 114504 (2007).

Figures

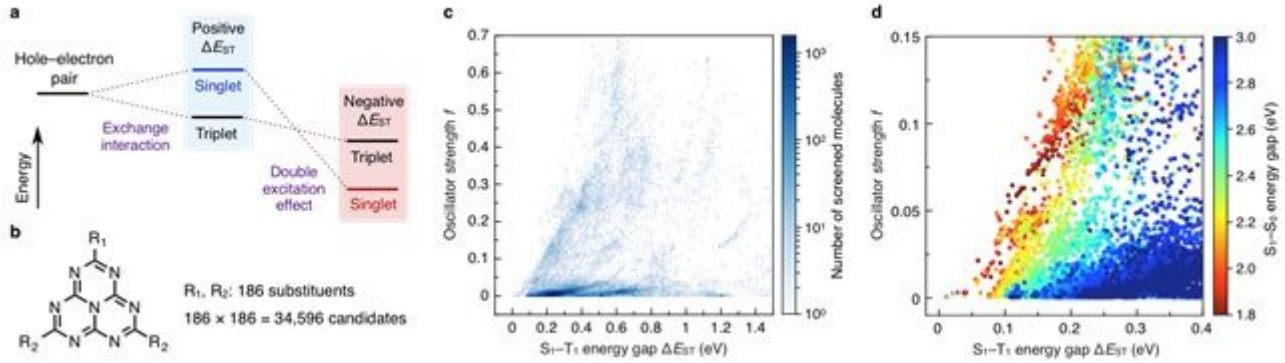

Figure 1

Computational screening of heptazine analogues. a, Schematic diagram of singlet and triplet excited states split in energy by the exchange interaction (middle) and then inverted by including the double-excitation effect (right). b, Molecular structures of the heptazine analogues examined in the computational screening. c, Number of screened molecules as a function of DEST and f calculated by TDDFT. c, S1–S0 energy gaps as a function of DEST and f calculated by TDDFT.

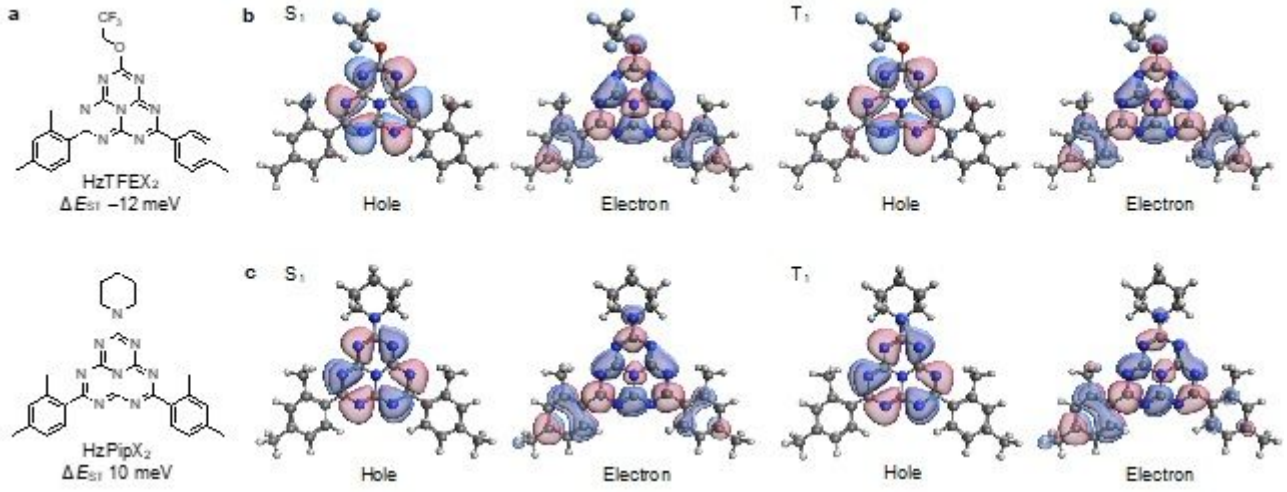

Figure 2

Lead candidate molecules HzTFEX2 and HzPipX2. a, Molecular structures of HzTFEX2 and HzPipX2 with EST calculated by EOM-CCSD. b, c, Dominant pair of NTOs of S1 and T1 of HzTFEX2 (b) and HzPipX2 (c) for the EOM-CCSD calculations.

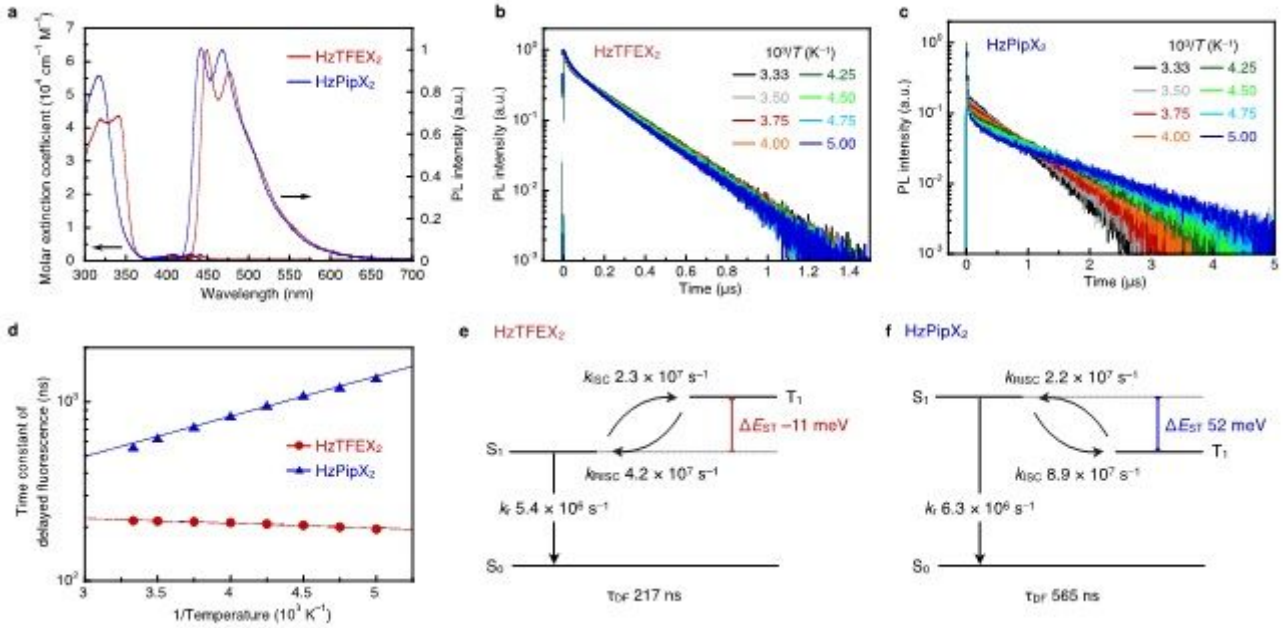

Figure 3

Photophysical properties of HzTFEX2 and HzPipX2 in deaerated toluene solutions. a, Steady-state absorption and PL spectra of HzTFEX2 and HzPipX2. b, c, Transient PL decay of HzTFEX2 (b) and HzPipX2 (c) at varying temperatures. d, Temperature dependence of tDF of HzTFEX2 and HzPipX2; the

solid lines in (d) represent the fits of tDF to a single exponential of inverse temperature. e, f, Schematic diagram of the excited states and the associated transitions of HzTFEX2 (e) and HzPipX2 (f).

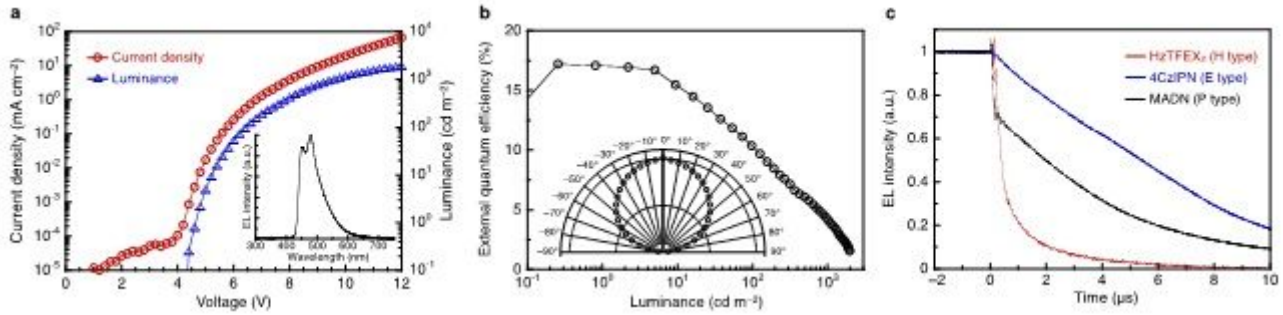

Figure 4

OLED performance. a, b, Current density–voltage–luminance characteristics (a) and external quantum efficiency–luminance characteristics (b) of the fabricated OLED using HzTFEX2; the inset in (a) shows the EL spectra measured at 1.0 mA, and the inset in (b) represents the viewing-angle dependence of the luminance almost consistent with the Lambertian distribution. c, Transient EL decays of the OLEDs using HzTFEX2, 4CzIPN, and MADN, respectively, measured in pulse operation with square-wave voltages of 8 V and −4 V.

Supplementary Files

This is a list of supplementary files associated with this preprint. Click to download.

- ExtendedData.pdf
- AizawaNatureESI.pdf